Review
Chinese Science Bulletin
SPECIAL ISSUE: New Energy Materials
November 2012 Vol.57 No.32: 4131–4142
doi: 10.1007/s11434-012-5409-3

Alternate redox electrolytes in dye-sensitized solar cells

LU JianFeng†, BAI Jie†, XU XiaoBao, LI ZhiHong, CAO Kun, CUI Jin & WANG MingKui*

Michael Grätzel Center for Mesoscopic Solar Cells, Wuhan National Laboratory for Optoelectronics, Huazhong University of Science and Technology, Wuhan 430074, China

Received October 30, 2011; accepted February 27, 2012

Dye-sensitized mesoscopic solar cell (DSC) has been intensively investigated as a promising photovoltaic cell. Redox electrolyte is important to determine the photovoltaic (PV) performance of the DSC devices, which has become the focus of this topic. In this contribution, recent advances in understanding and controlling of various redox couples are reviewed. Specially, we extend our discussion on the trends that enable iodide-free redox couples to be controllable and feasible for applications in the DSC with promising features.

solar cells, sensitizers, redox electrolytes, renewable energy, nanostructured materials, electrochemistry

Citation: Lu J F, Bai J, Xu X B, et al. Alternate redox electrolytes in dye-sensitized solar cells. Chin Sci Bull, 2012, 57: 4131–4142, doi: 10.1007/s11434-012-5409-3

1 Background

More and more people are realizing that the worldwide demand for energy has been massively increased and this situation will continue till a finial solution exists. However, several reports reveal that the production of oil, as one of the main energy sources, will soon be unable to keep up with the growing demand, thus leading to dire economic consequences. In order to sustain global political, economic and environmental stability, it is necessary to get an abundant supply of energy. Moreover, the development of carbon-free sources of energy becomes one of the major scientific challenges for us. As a potential alternative energy resource, solar energy has received extensive attention around the world after the energy crisis in 1970s [1]. Solar cells convert solar energy directly into electricity, which has become a major research interest within academia and industry. Approximately 90% of the PV units produced today are made from crystalline silicon (known as first generation solar cell), which is composed of large area p-n junctions, and others from thin films devices based on amorphous silicon (second generation solar cell, including CdTe, CIGS and other compound semiconductors). These devices based on p-n heterojunctions absorb part of the sunlight (absorption from 0.8–0.9 eV) and convert this light energy into electrical energy by the photovoltaic effect. Laboratory devices with efficiencies over 25% have been demonstrated, and the best commercial cells have now reached efficiencies of 17%–18% [2]. However, the high cost effectiveness of these devices still drives people to develop new type of solar cells expecting to possess high efficiency and low cost.

The dominance of the photovoltaic market by inorganic solid-state junction devices is now being challenged by the emergence of a third generation of cells. Among them the dye-sensitized solar cell (DSC, also known as Grätzel cell) with a new type of charge separation mechanism is a promising potential candidate [3]. The DSC, with a sandwich structure, is mainly composed of a mesoporous nanocrystalline network of wide band gap semiconductor (typically TiO_2), a monolayer of dye molecules (such as ruthenium dye) attached to the semiconductor, a redox electrolyte (typically I^-/I_3^-) and a platinum counter electrode. Figure 1 shows the basic structure and operating principle of the DSC. Basically, upon illumination, electrons in the sensitizer dye are photo-excited to be the excited states, followed by an electron injection into TiO_2 and electron diffusion through the mesoporous film and collection at the transparent

†These authors contributed equally to this work.
*Corresponding author (email: mingkuiw@yahoo.com)

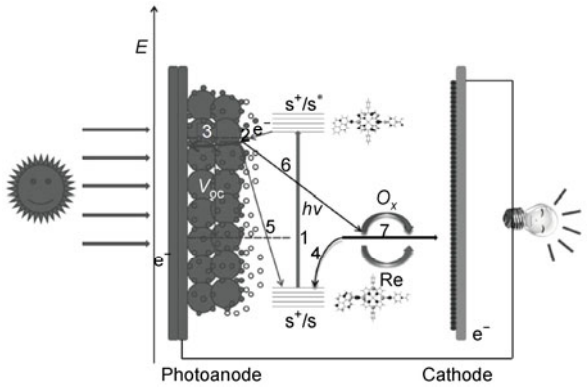

Figure 1 Schematic illustration of the electron-transfer processes occurring in the dye-sensitized heterojunction: process 1, light-induced excitation of the chromophore; process 2, electron injection into the conduction band of the TiO_2 semiconductor; process 3, electron diffusion in the TiO_2; process 4, dye regeneration via hole transporting medium; processes 5 and 6, the direct recombination of primarily separated charges and the secondary recombination process between the injected electron and the oxidized species in the hole transporting medium; process 7, charge transfer in the hole transporting medium.

conducting oxide (TCO) conducting glass. On the other hand, the photo-excited dye molecule will be regenerated by I^-/I_3^- redox system, which itself is refreshed at the counter electrode by the electron from the anode passing through the outer load.

At the heart of the DSC is a mesoporous oxide layer composed of nanometer-sized particles which have been sintered together to allow for electronic conduction to take place. The use of sensitizers having broad absorption band in conjunction with oxide film of nanocrystalline morphology permits to harvest a large fraction of sunlight. Thus, charge injection efficiency could be greatly improved by the strong chemical bonding between the absorbed dye and metal oxide semiconductor. Nearly quantitative conversion of incident photon into electric current is achieved over a large spectral range. The DSC cells can be fabricated with titanium oxide (TiO_2) nanocrystals that are coated with light-absorbing dye molecules and immersed in an electrolyte solution for manufacturing. This ease of production could possibly allow better manufacturability of this type of solar cell than others. The DSC cells have currently reached close to 13% efficiency under standard reporting conditions on the laboratory scale, while the efficiency of larger modules designed for outdoor conditions is attained at about 8%–10%. Though the DSC is still in relatively early stages of development, it shows great promise as inexpensive alternative to costly silicon solar cells and as attractive candidate for new renewable energy source [4,5].

Compared to conventional silicon based solar cells, the DSC can effectively produce electricity in low and diffuse light conditions. Like most PVs, the DSC can be easily directly integrated into the architecture of buildings. It is worthy to note that the DSC is the only solar cell that can be made truly transparent, the color depending on the choice of sensitizers. By selecting dyes that absorb only in the near IR and UV region it is even possible to produce colourless transparent windows. Figure 2 presents a DSC transparent panel with WNLO and MG center logos, which demonstrates the advantage of this technology.

In this report, we started with a review on the fundamentals of the DSC and solar cell operation. We then introduce the experimental tools to characterize the electrical properties of redox shuttles, followed with a review of the latest understanding in the domains of carrier transport, and surface passivation. We close with a detailed account of the latest research progress in performance and materials for the processing of organic redox electrolytes for the DSC.

1.1 Overview of materials, operational principles, and performance

In the DSC, the photoanode is generally composed of a TCO substrate coated with a high surface area nanocrystalline mesoporous TiO_2, which is sensitized with a broadly absorbing dye, such as $RuL_2(NCS)_2$ complex or $RuL(NCS)_3$ complex (several of them are presented in Figure 3) [6]. The most commonly used redox electrolyte in the DSC is iodide/triiodide (I^-/I_3^-) acting as a hole transporting material (HTM) [7]. The counter electrode is often platinum coated TCO, where the reduction of the redox mediator occurs to complete the electric circuit. The successes of the DSC comes from using the semiconductor with mesoporous structures with high surface area to replace the bulk one, 200–300 m^2/g nanocrystal TiO_2 as compared to approximately 10 m^2/g of flat single crystal, to provide a great enhancement for sensitizer loading and consequently, light harvesting efficiency.

After formation of the molecular excited state D^* of the dye (process 1 in Figure 1, eq. (1)) in light illumination, electron injection into the conduction band of the semiconductor $e^-_{TiO_2}$ (process 2 in Figure 1, eq. (2)) immediately takes place. The photon-injected electrons travel to the

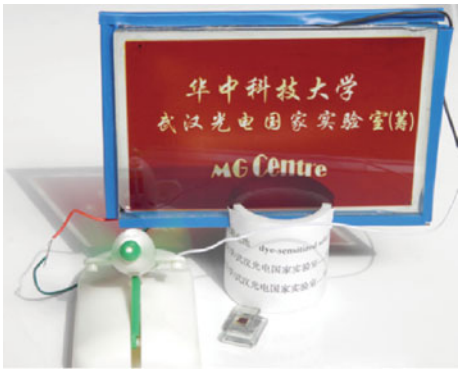

Figure 2 Dye-sensitized solar cell transparent panel with Michael Grätzel Center for Mesoscopic Solar Cells (MG Center), Wuhan National Laboratory for Optoelectronics (WNLO), and Huazhong University of Science and Technology (HUST) logos.

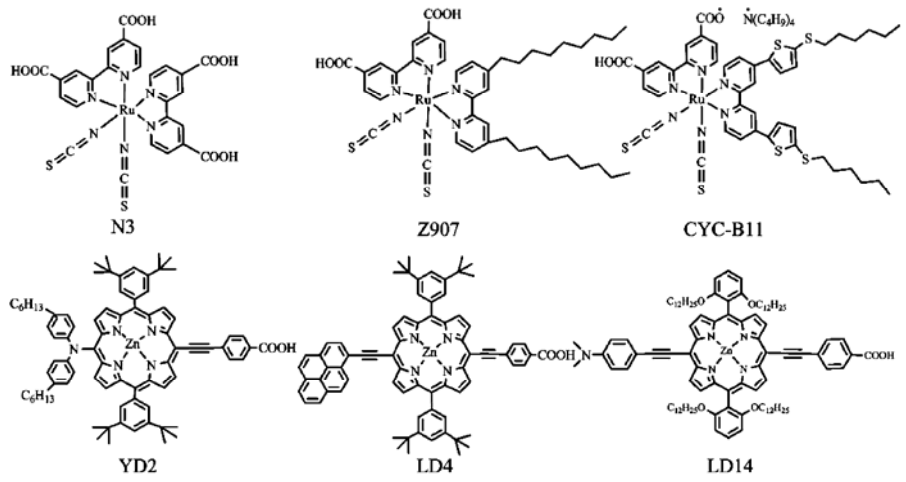

Figure 3 Structures of ruthenium and porphyrin dyes.

counter electrode via the external circuit to reduce the oxidized species form of the redox shuttle species O_x (process 7 in Figure 1, eq. (3)) in the electrolyte, and oxidized dye, D^+, is regenerated to its chromophoric form D by the reduced species of the redox shuttle Re (process 4 in Figure 1, eq. (4)) to complete the cyclical process with no net chemical reaction.

$$D + h\nu \longrightarrow D^* \qquad \text{process 1} \qquad (1)$$

$$D^* \longrightarrow D^+ + e^-_{TiO_2} \qquad \text{process 2} \qquad (2)$$

$$O_x + e^-_{cathode} \longrightarrow Re \qquad \text{process 3} \qquad (3)$$

$$D^+ + Re \longrightarrow D + O_x \qquad \text{process 4} \qquad (4)$$

There are two energy-wasting possibilities for an injected electron ($e^-_{TiO_2}$). One possibility involves the recombination of the electron with the oxidized sensitizer (D^+) and converting it back to ground state dye (D), also called as back electron transfer (process 5 in Figure 1), shown in the following equation:

$$D^+ + e^-_{TiO_2} \longrightarrow D \qquad \text{process 5} \qquad (5)$$

The second energy loss channel involves reduction of the oxidized species in the HTM (process 6 in Figure 1, eq. (6)) at the bare TCO or on the wide band-gap semiconductor nanoparticles surface instead of the counter electrode.

$$O_x + e^-_{TiO_2} \longrightarrow Re \qquad \text{process 6} \qquad (6)$$

1.2 Basic diode model of a DSC

The DSC equivalent circuit and classic current-voltage (*J-V*) curve are presented in Figure 4. The overall solar conversion efficiency, η, is a product of the short circuit current (J_{sc}), the open circuit voltage (V_{oc}), and the fill factor (*FF*, expresses the shape of the *J-V* curve), according to:

$$\eta = \frac{J_{sc} \times V_{oc} \times FF}{P_{in}}, \qquad (7)$$

where P_{in} is the total solar power incident on the cell at air mass (AM 1.5) 100 mW cm^{-2} illumination intensity.

Generally, the *J-V* characteristics of a photovoltaic device can be described by the following equation according to the basic diode model.

$$J = J_{ph} - J_0 \left[\exp\left(\frac{q(V + JR_s)}{mk_BT} \right) - 1 \right] - \frac{V + JR_s}{R_{sh}}, \qquad (8)$$

where J_{ph} is the photocurrent modelled as a current source, J_0 is the reverse saturation current (dark current) of the diode, q is the electron charge, m is the diode ideality factor, and R_s and R_{sh} are the series and shunt resistances of the cell.

The influence of different elements can be evaluated by simulating *J-V* characteristics of the DSC. Partial results are presented in Figure 4. We first evaluate the influence from R_s and R_{sh} on the photovoltaic performance. R_s is the sum of the film resistance, electrode resistance, and the contact between the film and the electrode. R_{sh} is mainly associated with carrier recombination loss, being related to the leakage of the current. As demonstrated in Figure 4(a), increasing the series resistance R_s reduces primarily the *FF*, followed by the J_{sc}, but has no effect on V_{oc}, when keeping other parameters constant, while the shunt resistance, R_{sh} has little influence on the V_{oc} and J_{sc}, but on the *FF* (Figure 4(b)). A large drop in R_{sh} collapses the device performance. The ideality factor m value of TiO_2 film has an effect on the *J-V* characteristics of the DSC (Figure 4(c)), showing that when m increases (meaning a highly rectifying diode), the J_{sc} is almost constant, but V_{oc} and *FF* increases significantly. The reverse saturation current, J_0, has an obvious effect on the V_{oc} (Figure 4(d)). A reduction in the value of J_0 results in increasing the V_{oc}, due to an enhancement in the charge separation at the oxide electrolyte interface. The V_{oc} is related to the interfacial charge recombination process

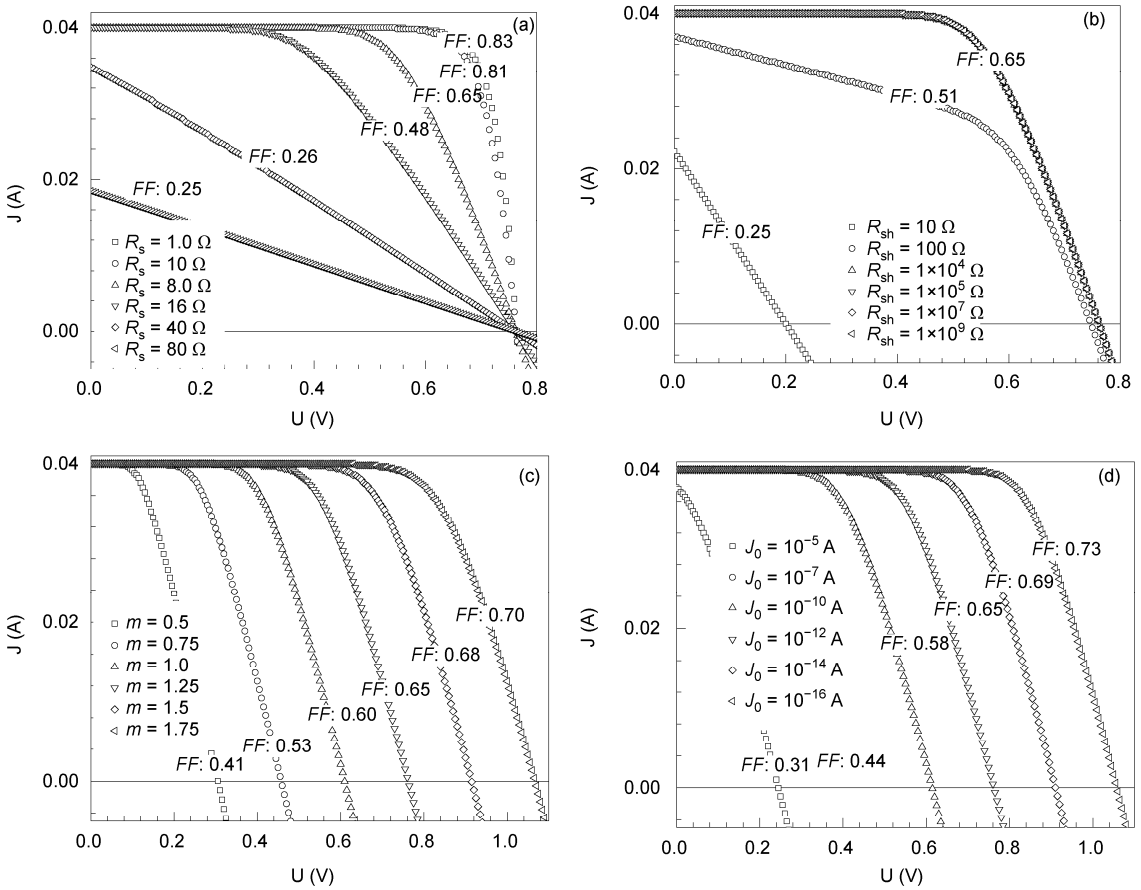

Figure 4 Simulation results based on the eq. (8) according to the basic diode model as discussed in the text. The influence from (a) R_s, series resistance; (b) R_{sh}, shutting resistance; (c) m, the diode ideality factor; and (d) J_0, the reverse saturation current (dark current) of the diode on the *J*-*V* curve of the DSC device.

between the dye-sensitized heterojunction and electrolyte. At open circuit conditions, all photo-generated carriers recombine within the solar cell diode [7]. Thus, if recombination can be minimized, V_{oc} can approach more closely to the maximum values. From Figure 4, we can conclude that the larger value of R_{sh} and m, and small values of R_s and J_0, can lead to a device with good *FF*, thus enhancing the power conversion efficiency.

1.3 Overview of improvement efficiency of a DSC

The best method for improvement efficiency of the DSC is to enhance J_{sc}, V_{oc}, and/or *FF*. Clearly, the most straightforward way to increase J_{sc} is to absorb a greater fraction of the incident light. The optical gap of the Ru complex in the most efficient DSC to date is about 1.8 eV, allowing it to absorb essentially all the light up to ~700 nm. Increasing the photocurrent density requires decreasing the optical gap to extend the dye's absorption into the near infrared [7–10].

Recent improvements in the design and synthesis of new dyes have made it possible to obtain devices with light-to-energy conversion efficiencies greater than 12%. Xie et al. [11] have reported an up-conversion luminescence powder TiO_2 (Er^{3+}, Yb^{3+}), converting infrared light which the dye cannot absorb, into visible light with wavelengths of 510–700 nm which the dye can absorb, thus increasing the photocurrent of the DSC. Several ruthenium complexes (as presented in Figure 3) [12–14] and donor–acceptor-substituted porphyrins (as presented in Figure 3) [15–17] have been developed and investigated intensively as photo-sensitizers via excitation of the metal to ligand charge transfer (MLCT) transition. Taking the well developed ruthenium complex as an example, its ligands can be modified by inserting electronic moieties between each hydrophobic alkyl chain and the 2,2-bipyridine ring, which can tune both the LUMO and the HOMO levels of the complex. Therefore, effectively injecting the electrons into the conduction band of the titania and transferring the holes to the redox species, can be expected. This strategy has proved to be a viable route for developing new efficient photo-sensitizers [18]. From the view of cost, among the non-Ruthenium based dyes, porphyrins have attracted considerable attention as the light harvesting antenna unit. To date, most of porphyrin sensitizers for the DSC application have D-B-A structure, in which B represents a π-conjugation bridge serving as a spacer between the porphyrin light-harvesting center D and the anchoring group A. Very recently, these push–pull zinc porphyrin sensitizers were designed, synthesized and char-

acterized for highly efficient green see-through photovoltaic applications. Lu et al. [19] found that elongation of the π-conjugation and loss of symmetry in porphyrins can broaden the photo response range with an increasing intensity of the Q bands relative to that of the Soret band. Thus, the performance of porphyrins based cells has disclosed a remarkably high power conversion efficiency that was close to that of the ruthenium complexes, which could be attributed to broader and more red-shifted spectral feature that makes the incident photon to current efficiency (IPCE) spectrum to cover broadly across the entire visible region (400–800 nm).

Usually, chemists would take two methods to narrow the dye's optical gap: either to lower the energy of the LUMO or to raise the energy of the HOMO. Obviously, moving the ground-state potential negatively is better than that of shifting the dye's excited state potential positively, in order to keep the photo-induced electrons injected efficiently into the conduction band of the semiconductor material [12–14,19,20].

The V_{oc} given by a DSC device is approximately equal to the energy difference of nanocrystalline TiO_2 Fermi level and that of the redox couple electrolyte. Thus, a redox couple with higher redox potential principally can take a higher photo-voltage. As discussed in Section 1.4, there is only a little room for an improvement of *FF*. Therefore, a fine optimization on the composition of redox is critical to the efficiency improvement of the DSC, mostly through the increase in photo-voltage of the device. It is important to note that the total series resistance of the cell attenuates the *FF*.

1.4 Critical requirements on redox electrolytes

The key function of redox electrolytes in the DSC is to transfer electrons to the oxidized sensitizer dye molecules that are formed photochemically via electron injection into TiO_2, completing the internal electrochemical circuit between the photoanode and the counter cathode (processes 4 and 7 in Figure 1). The dual criteria of fast dye regeneration and slow interception place a challenging constraint on identifying effective redox shuttles. The interception of the oxidized dye by the reduced species of the electrolyte is also crucial for obtaining good conversion yields and high cycle lifetime of the sensitizer. Thus, the redox couple presented in the electrolyte is of crucial important for stable operation of the DSC. The conventional DSC employs a liquid electrolyte (usually an iodide/triiodide redox active couple dissolved in an organic solvent). A scientifically interesting and promising approach to replace the liquid electrolyte is the use of quasi-solid electrolyte, and solid-state electrolyte as well as p-type semiconductors (referred as HTM).

The redox couples in the electrolyte affect the DSC's performance, mainly on the photovoltage. An ideal redox shuttle with the redox level closer to the D^+/D redox level is critical so as to increase the V_{oc} while still maintaining rapid regeneration of the dye to prevent degradation. Furthermore, those performance can also be affected by non-electroactive species applied in different electrolytes, for example some small cations (such as protons, Li^+), organic cations (such as dialkylimidazolium), or additives (such as 4-tert-butylpyridine tBP) [21–24]. While several previous studies have explained the effect of the electrolyte composition on the photovoltaic performance of the DSC, many questions still remain open to date.

2 Advantages and disadvantages of iodide/iodine based electrolytes

Up to now, I^-/I_3^- electrolytes have been demonstrated to be one of the best cases, which have ideal kinetic properties that lead to an "asymmetric behavior" at the basis of the efficient functioning of the DSC: the forward electron donation by I^- is a facile mono-electronic process, which ensures an efficient dye recovery (k_{REG} in Figure 1), while the reduced specie appears to be largely inefficient allowing for a minimization of the interfacial back recombination. Though it shows remarkable performance in the DSC, the interest in finding suitable alternatives is still strong due to number of reasons: light adsorption by I^-/I_3^- couple in the visible range, severe corrosion of I_3^- to several materials, and a mismatch (about 0.6 V) between the redox potential of the sensitizer cation D^+ ($E_{F,redox} \approx 1.0$ V vs. NHE) and that of I^-/I_3^- ($E_{F,redox} \approx 0.4$ V vs. NHE). Furthermore, one of problems that have not yet been solved is to create an economic and durable encapsulation technology to increase the lifetime of iodide based DSC device.

Several attempts have been made to find a suitable alternative to the I^-/I_3^- system, such as Co^{2+}/Co^{3+} complexes containing electrolytes, organic and inorganic hole transporting materials and polymer based electrolytes. The literatures investigation on redox shuttles for DSC application shows there are no redox couples permitting to maximize the device energy conversion efficiency. Therefore, it is highly desired to have new redox couples with improved properties. The targeted redox couples principally should have attractive physical and chemical properties, such as good solubility, substantially colorless or be substantially optically clear at concentrations permitting a good conductivity, a low vapor pressure, a high thermal stability, no corrosion to components when used in a device. Additionally, a good redox couple has a small ΔE_p, which is an indication of the high degree of reversibility.

3 Methods for redox couple studies

Several techniques have been employed to investigate the redox shuttle related kinetic dynamics, including intensity modulated photovoltage spectroscopy (IMPS), charge extraction, photovoltage and photocurrent transients decay, scanning electrochemical microscopy, electrochemical im-

pedance spectroscopy (EIS), transient absorption spectroscopy (TAS), and photoinduced absorption spectroscopy (PIA) measurement of the oxidized dye and electrons in the semiconductor provide information of the photoexcited electron injection process, etc. Nanosecond-millisecond TAS has been applied to evaluate the electron-transfer dynamics in the DSC with various electrolytes. EIS has been developed widely to study the interfacial kinetic processes, mostly in dark conditions. The small amplitude techniques intensity modulated photovoltage spectroscopy (IMVS) and intensity modulated photocurrent spectroscopy (IMPS) are suggested to capture the respective time constants for charge recombination at open circuit and the combined processes of charge collection at short circuit in the DSC. During photo-voltage and photocurrent transient decay measurements, by monitoring the relaxation of the studied devices back to the steady-state at open circuit following a transient perturbation produced by a weak probe pulse, can give the information on the characteristic electron lifetime for recombination. Similarly, the photo-current transient decay and the photovoltage rise time at short circuit provide information on the electron transport rate within titania film. Recently, scanning electrochemical microscopy (SECM) was applied to study the charge transfer kinetics between I^- and photo-oxidized dye molecules (Eosin Y^+) adsorbed on ZnO film [25].

4 Iodide/iodine free redox couple as electrolytes of a DSC

4.1 Transition metal complexes systems

Alternative one-electron outer sphere redox shuttles of transition metal complexes show promising potential in DSC application. Nusbaumer et al. [26] have studied on cobalt polypyridyl complexes (Figure 5) in combination with ruthenium dyes for DSC application and demonstrated an impressive efficiency of over 8% at low light intensities. Further investigation revealed a large recombination due to a fast reduction of the oxidized species (Co^{III}) taking place at the TCO/electrolyte interface. The low photocurrent at full sunlight intensity was observed, which could be attributed to the diffusional limitation caused by the big molecular size of redox shuttle.

Feldt et al. [27] have designed several organic dyes and cobalt polypridine redox mediators for highly efficient DSC (see Figure 5). The DSC having efficiencies surpassing the record for those with iodide-free electrolytes was developed by selecting a suitable combination of a cobalt polypyridyl complex and an organic sensitizer. Solar cells with overall conversion efficiencies of 6.7% and open circuit potentials of more than 0.9 V under standard 1 sun intensity condition was obtained by utilizing a triphenylamine-based organic dye in combination with tris(2,2′-bipyridyl) cobalt$^{(II/III)}$. The authors concluded that the augmented overall device performance was attributed to the steric properties of triphenylamine based organic sensitizers and cobalt polypyridyl redox mediators, thus to the fast charge transport and reduced recombination processes. Excellent performance was also found under low light intensity indoor conditions. With the same strategy, in combination with an announced new donor-acceptor organic sensitizer such as bearing with 2,6-bis(thiophen-2-yl)-4,4-dihexyl-4H-cyclopenta[2,1-b:3,4-b0] dithiophene-conjugated spacer or cyclo-pentadithiophene bridging unit in the D-π-A structure with cobalt$^{(II/III)}$ redox shuttle, highly efficient DSC (over 9.0%) were reported by different groups [28]. These systems generate high power conversion efficiency performance which can be mainly attributed to the specific molecular design of organic dyes greatly retarding the rate of recombination (process 6 in Figure 1), thus enhancing photo-voltage.

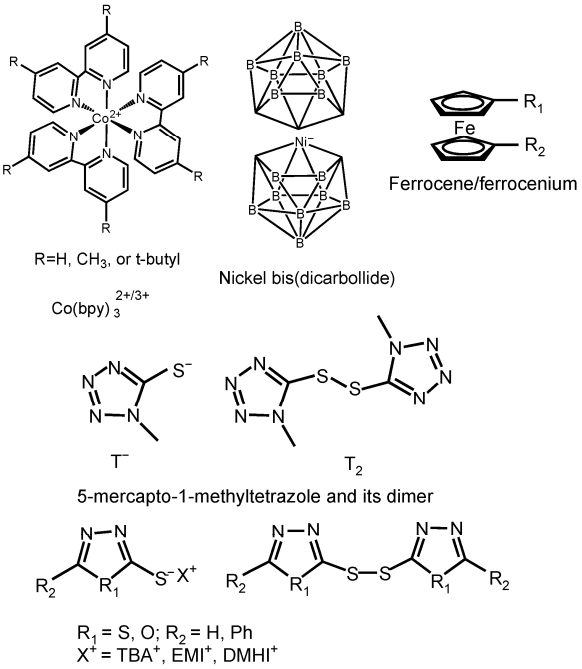

Figure 5 Various redox shuttles used in DSCs.

Li et al. [29] have reported a promising new class of $Ni^{III/IV}$ bis(dicarbollide) complexes (see Figure 5) as a fast, non-corrosive redox shuttle for the DSC application, therewith a framework with electron donating and electron withdrawing groups. The authors have demonstrated that through chemical modification of the Ni-bis(dicarbollide) moiety in the B(9/12) positions, the $Ni^{III/IV}$ redox pair potential can be systematically tuned over a 200 mV range, overlapping the I^-/I_3^- redox couple. The DSC can be benefit from this shuttle. Although the entire scope is not yet explored, this work offers an avenue to create diverse redox couples for DSC application, yielding valuable fundamental information concerning device function [30].

The one electron, outer-sphere redox shuttle ferrocenium/ferrocene (Fc^+/Fc) couple had been intensively investigated in the DSC filed due to its favourite kinetics property.

Previously result disclosed that Fc^+/Fc couple is not suitable electrolytes for DSC application due to a facile back transfer of electrons from the TiO_2 and the substrate. In order to retard the unexpected recombination, various technologies have been used, such as atomic layer deposition, to produce surface coatings onto the nanoporous films. But the results were not satisfied due to the dilemma of injection and recombination [31]. Very recently Daeneke et al. [32] have reported a highly efficient DSC based on the Fc^+/Fc couple in combination with a carbazole donor-acceptor organic dye. An addition of co-adsorbent into the dye solution can further improve the device performance. An impressively high open-circuit voltage under AM1.5 conditions (842 mV) with a short circuit current of 12.2 mA cm^{-2} was achieved, yielding an energy conversion efficiency of 7.5%. The respectable performance was attributed to a reduction of the HOMO-LUMO gap of dye molecules, which leads to faster dye regeneration and electron injection processes as discussed above.

4.2 Solid-state hole transporting materials

Replacement of the liquid electrolyte in DSC devices by a solid-state charge-carrier material helps to avoid problems encountered with evaporative solvent loss by escape through pinholes in the sealing. These solid-state HTMs can be crystalline inorganic salts, such as CuI and CuSCN, or amorphous organic molecular solids and polymer, such as those based on triaryamine derivatives 2,2′,7,7′-tetrakis(N, N-di-p-methoxy-phenylamine)-9,9′-spirobifluorene (spiro-MeOTAD) and N,N′-diphenyl-N,N′-bis(3-methylphenyl)-(1,1′-biphenyl)-4,4′-diamine (TPD). The initial successful demonstration of the feasibility of making SSDSC devices reported in 1998 announced a 0.74% power conversion efficiency. SSDSC devices with high efficiency have been reported when using amphiphilic heteroleptic ruthenium sensitizers with high molar extinction coefficients [33]. The improved efficiency can be attributed to the self-assembly of such dyes, forming a dense layer onto the surface of TiO_2 nanoparticles, which augments the light harvesting efficiency and interfacial charge recombination lifetime. Yue et al. [34] have utilized blend heterojunction consisting of C_{60} derivatives [6,6]-phenyl-C61-butyric acid methyl ester (PCBM) and poly(3-hexylthiophene) (P3HT) as charge carrier transferring medium to fabricate flexible DSC devices. The PCBM/P3HT heterojunction has not only the absorption in ultraviolet light for PCBM, but also the absorption in visible and near infrared light for P3HT, which widens the photoelectric response range of the DSC. Overall 1.43% power conversion efficiency was achieved under 1 sun illumination condition. In order to get favourable interaction between the HTM and the dye-coated surface, an amorphous "liquid" organic semiconductor was synthesized and applied successfully as a hole transporting material in the DSC. The resulted DSC devices exhibited power conversion efficiencies close to 2.4% under simulated air mass 1.5 solar spectrum at 100 mW cm^{-2}, and incident photon-to-electron quantum efficiencies in excess of 50% [35]. The charge transport properties and mechanisms of the "liquid" organic semiconductor show similarity to their solid-state counterparts.

4.3 Organic redox shuttles

Recently Wang et al. [36] have reported the possibility of using of a thiolate/disulfide-based redox couple that has interesting properties. The reported reodx shuttle is 1-methy-1H-tetrazole-5-thiolate (T^-) and its dimmer (T_2) redox couple (see Figrue 5). Electrolytes based on this redox couple have almost no adsorption in the visible part of the spectrum. Its similar redox potential with that of the I^-/I_3^- redox couple, its better dissociation in organic media and its much less intense coloration are responsible for the significant increase of the device energy conversion efficiency. The advantage of employing this organic redox shuttle is the ability to increase the photon harvesting capacity for the devices. The IPCE of devices A, B and C are shown in Figure 6(a). Compared to device C (I^-/I_3^- based), device A (with T^-/T_2 as a redox couple without additives) has a broader IPCE in the spectral range 360–460 nm. From wavelengths 360 to 460 nm an increase in the integrated

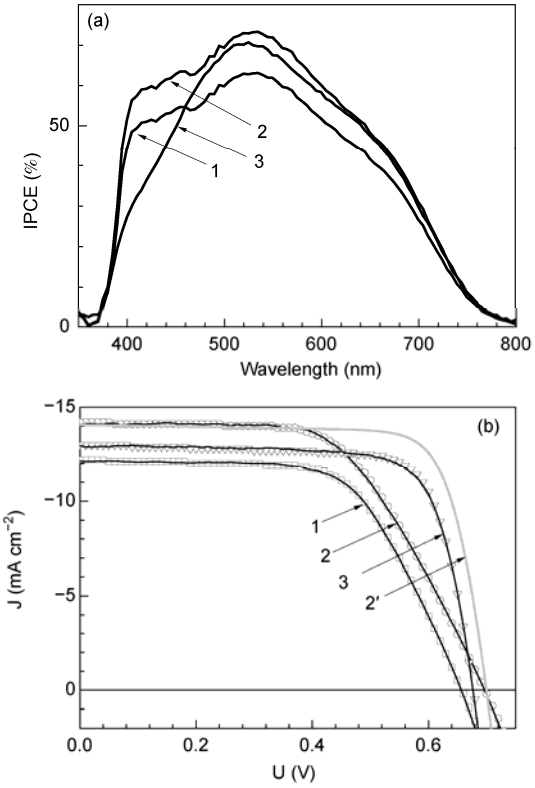

Figure 6 (a) IPCE and (b) *J-V* characterization of various devices. 1, Device A; 2, Device B; 3, Device C; 2′, simulation Device B by reducing the R_S.

Table 1 Photovoltaic parameters of various devices and the electric elements obtain by fitting the *J-V* curve with the simple diode model

	V_{oc} (V)	J_{sc} (mA cm^{-2})	*FF*	η (%)	J_{ph} (mA cm^{-2})	*m*	R_s (Ω)	R_{sh} (Ω)	α
T-based electrolyte (Device A)	0.656	12.166	0.63	4.99	12.1	1.11	11.52	1430	0.46
T-based electrolyte with additives (Device B)	0.969	14.231	0.58	5.79	14.1	1.16	13.39	1910	0.33
Iodine based electrolyte (Device C)	0.676	12.81	0.75	6.48	13	1.14	2.15	1080	0.38
T-based electrolyte with additives[a)]	0.698	14.06	0.78	7.62	14.1	1.16	2.15	1910	

a) Relevant photovoltaic parameters derived from fitted *J-V* curves shown in Figure 6(b) (the efficiency is based on an illumination power density of 100 mW cm^{-2}).

current (2.03 vs. 1.49 mA cm^{-2}) between devices A and C of 36% was obtained, which clearly shows the advantage of this redox couple. This could be attributed to a much lower light absorption of the new redox couple compared to that of I^-/I_3^-. The presence of additives (4-tert-butylpyridine tBP and Li^+) in electrolyte enhanced the photovoltaic performance of device B to 5.8% (Figure 6(b), Table 1). By increasing the thickness of the 20 nm titania transparent film from 8 to 11 μm in a double-layer structure, the efficiency was further improved to 6.44% [36]. From Figure 6, one can infer that the devices utilizing the new organic redox couples have lower fill factor comparing to that of I^-/I_3^-. The *J-V* curves can be fitted by using the model with eq. (8) as discussed above. The fitting results are presented in Table 1, showing that the charge transfer resistance (included in the series resistance R_s) of the new shuttle at the counter electrode is 5 times larger than that of I^-/I_3^- case. This large R_s diminishes fill factors. If the R_s in the case of new redox shuttle can be reduced to a value similar to that of I^-/I_3^-, an augmented device efficiency (from 5.8% to 7.6%) could be obtained, principally due to the increase of fill factor (see Figure 6(b) and Table 1).

EIS was used to study the interfacial recombination kinetics. Figure 7(a) shows the impedance spectra at a bias of –0.725 V of Device A serving as an example in the dark. The resulting frequency analysis typically shows three well separated semicircles in the Nyquist diagram. In the order of increasing frequency these are attributed to the Nernst diffusion of the redox mediator within the electrolyte (III, Figure 7(a)), the electron transfer at the oxide/electrolyte interface as well as their diffusion in the nano-particle network (II, in Figure 7(a)), and the electrochemical reaction at the counter electrode (I, Figure 7(a)). The electron transport process and charge recombination dominate the impedance spectra upon lowering the bias. Several physical models have been proposed to understand all the complex charge-transfer processes that take place in the DSC, in which the transmission line model (Figure 7(b)) attracts most of the attention. Two parallel charge transport channels, representing a) electron transport through the TiO_2 and b) hole transportation in the HTM within the pores, are the fundamental parts of the conceptual model (Figure 7(b)). In this model, an extended distributed element (DX in Figure 7(b)) was introduced to interpret the impedance due to the diffusion of electrons and holes and their recombination across

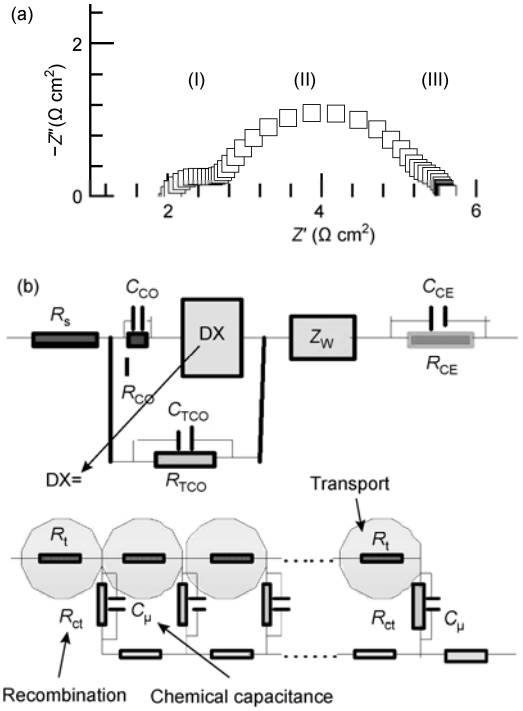

Figure 7 (a) The impedance spectroscopy curve of Device A measured in dark at the bias of –0.725 V and (b) finite length transmission model used in this text to fit impedance spectroscopy.

the dye sensitized heterojunction.

Using the transmission line model, the important elements, such as electron diffusion resistance (R_t) and recombination resistance (R_{ct}) are derived by fitting the impedance data, thus the apparent recombination lifetime (τ_e, $\tau_e=R_{ct}C_\mu$) can be obtained. The electron transfer resistance depends on the density of electrons (n_{cb}, $n_{cb}=N_{cb}\exp((E_{F,n}-E_{cb})/(k_BT))$ in the conduction band (CB) and mobility (μ_e, the free electrons diffusion coefficient $\mu_e=(D_e q)/(k_BT)$ according to the Einstein relation on diffusion of charged particles). The resistance R_t can be described by eq. (9).

$$R_t = \frac{k_B T N_{cb}}{q^2 D_e}\exp\left(-\frac{E_{F,n}-E_{cb}}{k_B T}\right) = R_0 \exp\left(\frac{E_{cb}-E_{F,redox}}{k_B T}\right)\exp\left(-\frac{U}{k_B T}\right), \quad (9)$$

where R_0 ($R_0=(k_BTN_{cb})/(qD_e)$) is film resistance at the applied bias ($U=E_{F,n}-E_{F,redox}$) where the electron Fermi level

($E_{F,n}$) matches the conduction band edge (E_{cb}), and $E_{F,redox}$ is the equilibrium potential of redox couple in the electrolyte. In eq. (9), the first term on the right hand side represents the influence from charge mobility related to the trapping and de-trapping of electrons from states in the band gap, second term being the influence from the position of the lower edge of the conduction band (CB), and third term being from the applied potential on the sensitized TiO_2 electrode, respectively. Figure 8(a) presents the effect of the applied voltage U (U=$E_{F,n}$–E_{redax}) on the electron transport resistance R_t under dark condition for the various devices. The logarithm of the electron transport resistance presents parallel behavior for various devices. The electron transfer resistance depends on the density of electrons (n_{cb}) in the CB and the mobility (μ_e, the free electrons diffusion coefficient according to the Einstein relation on diffusion of charged particles). Thus, the shift of the resistances for the steady state electron transport in those devices is attributed to a change in position of the conduction band edge (E_{cb}) and/or the free electron mobility (μ_e). The R_t data from the device using T^-/T_2 redox are shifted downward (–67 mV) from those of the device using I^-/I_3^- redox, which is mainly caused by a difference (about 51 mV) in redox potential of these two couples. A further negative shift (27 mV) of E_{cb}, relative device using I^-/I_3^- redox, was seen for the device using T^-/T_2 with tBP and Li^+ as additives, which is generally observed in the case of solar cells.

Another important element, the chemical capacitance C_μ, thus can be extracted from impedance measurement. The chemical capacitance is defined as the amount of electronic charge necessary for increasing the Fermi level of the nanocrystalline oxide film by 1 eV. The chemical capacitance presents the electronic level for electrons or hole transport in the charge carriers, the energy levels for the interfacial charge transfer as well as giving a reference for conduction band position. Considering the variation of both free and localized electrons as discussed above, the chemical capacitance of electrons in the DSC can be expressed as follow:

$$C_\mu = e^2 \frac{\partial(n_c + n_1)}{\partial \mu_n} = C_\mu^{cb} + C_\mu^{trap}. \quad (10)$$

The first term in eq. (10), (C_μ^{cb}), due to the free electrons in the conduction band can be obtained by

$$C_\mu^{cb} = e^2 \frac{n_c}{k_B T}. \quad (10a)$$

The second component, (C_μ^{trap}), related to the contribution of localized electron trapping states to the chemical capacitance can be expressed as

$$C_\mu^{trap} = e^2 \frac{\partial n_t}{\partial E} = e^2 \int_{E_2}^{E_1} f(E - E_F) \cdot g(E) dE \approx e^2 g(E). \quad (10b)$$

The rise of chemical capacitance as a function of applied bias shows the expected exponential behavior for this parameter in the mesoscopic TiO_2 films (see Figure 8(b)). The devices using new redox shuttle with additives exhibit higher chemical capacitance of trapped states than that of device C with I^-/I_3^- at the same bias. The exponential distribution of trap states can be described with the characteristic parameter T_0, as presented in eq. (10b). We introduce another parameter α ($\alpha = T/T_0$). The parameter α is a dimensionless quantity of a specific material. Normally, smaller α corresponds to a steeper trap state distribution. One can obtain the value of parameter α by fitting the curves in Figure 8(b) with a biexponential function, to be 0.36, 0.33, and 0.38, respectively, corresponding to device A, B and C.

The product of the recombination resistance (R_{ct}) with the chemical capacitance (C_μ) yields the apparent electron lifetime (τ=$R_{ct}C_\mu$). Results for various charge density values are presented in Figure 8(c) (empty circuit symbols). Device C has the shortest apparent electron lifetime at a given electron density among the tested samples. From the apparent

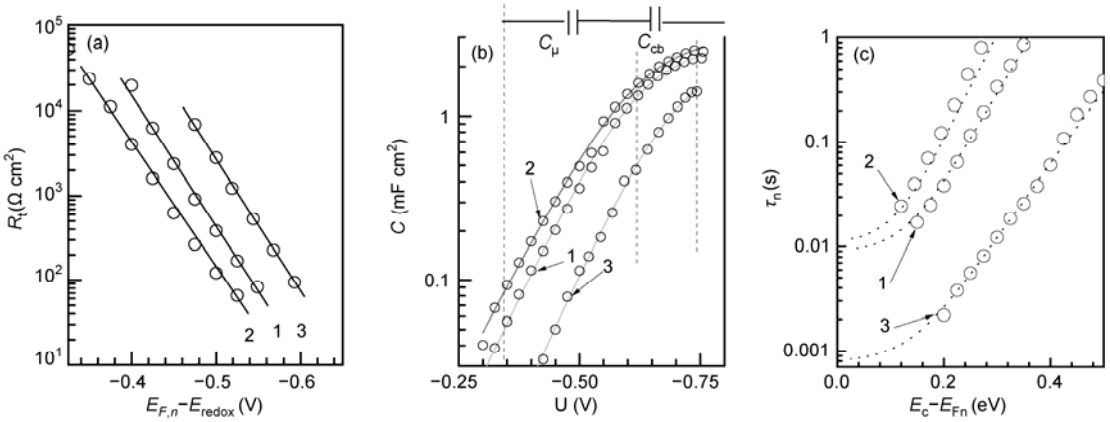

Figure 8 (a) Electron transporting resistance R_t and (b) chemical capacitance C from impedance measurements in dark as a function of the bias, and (c) apparent recombination lifetime τ from impedance measurement in dark as a function of the electron Fermi level offset with respect to the conduction band edge. The dotted line are the fitting results from eq. (12). 1, Device A; 2, Device B; 3, Device C.

electron lifetime, the conduction band electron lifetime and the charge transfer rate constants can be determined as discussed below.

In order to better understand the charge recombination dynamics of various redox shuttles at the dye-sensitized heterojunction interface, we have modeled the electron-hole recombination procedure by considering the continuous-time random walk of electron transport in a trap-dominated material. According to the quasi-static treatment, the apparent charge recombination lifetime (τ_n) under different energy levels is related to the conduction-band electron lifetime (τ_0) by using the following expression:

$$\tau_n = \tau_0 \left(1 + \frac{\partial n_t}{\partial n_c} \right), \tag{11}$$

where n_t is the trapped electron density, τ_0 is the inverse of the pseudo first-order rate constant for the back transfer of electrons from the conduction band, and n_c is the conduction band electron density. It is reasonable to assume that these levels are associated with surface states present at the high internal surface area of TiO_2 nanoparticles or with trapping levels at the particle–particle contact. Thus, eq. (11) can be expressed by

$$\tau_n = \tau_0 \left[1 + \frac{N_{t,0}}{N_c T_0} \exp\left(\frac{E_{cb} - E_{Fn}}{k_B T} \right)^{(T_0 - T)/T_0} \right], \tag{12}$$

where $N_{t,0}$ and N_c are the total density of the localized states and the accessible density of states in the conduction band; others have the normal physical meaning. The measured apparent charge recombination lifetime τ_n differs substantially from the free electron lifetime (τ_0) and is dependent on the trap occupational level. The conduction band electron lifetime (τ_0) and the apparent charge recombination lifetime (τ_n) can be evaluated with eq. (12).

In order to fairly compare those lifetimes at an equal electron concentration in the titania nanoparticles, the difference between the conduction-band edge and the Fermi level, that is, E_c–E_{Fn}, is used in Figure 8(c) as abscissa instead of the applied forward bias voltage (U). We note the apparent recombination lifetime τ_n decreased for the device B (with additives of Li^+ and tBP) compared to that of the device A (without additives) at an identical energy offset. Device C has the shortest electron lifetime (τ_n) at a given electron Fermi level offset. By using eq. (12), the fit to the data in Figure 8(c) gives conduction band electron lifetimes (τ_0) of 9, 11, and 0.8 ms for devices A, B, and C in the dark, respectively. Since the concentration of oxidized species is same for different shuttles (0.4 mol/L) in the calculation of the rate constants and the same solvent is used, it can be concluded that the recombination kinetics was depended on the shuttle itself. The interfacial recombination mostly takes place between those electrons trapped by surface state with the oxidized state of new redox shuttles. However, the recombination might be mainly contributed from electrons in the conduction band for I^-/I_3^-.

Tian et al. [37,38] have synthesised a series of organic thiolate/disulfide redox couples and systematically studied in the DSC based on an organic dye. The poly(3,4-ethylenedioxythiophene) material has been used as the counter electrode in this kind of iodine free DSC devices showing a promising efficiency of 6.0% under AM 1.5 G light illumination. Ning et al. [39] have reported 2-mercapto-5-methyl-1,3,4-thiadiazole derivatives pure organic redox couple for quantum dot sensitized solar cells. They found that this pure organic electrolyte shows not only a significantly reduced charge recombination, but also the advantage of avoiding the metal corrosion character of the iodine electrolytes. All these characteristics make it a promising electrolyte candidate for quantum dot sensitized solar cells.

4.4 New architectures for the DSC

Recently, implementation of an active photocathode with a photoanode opens the possibility to fabricate tandem DSC devices. In this case the organic redox couple electrolyte is very promising for utilization in p-type DSC device, if considering the advantage of transparent fast diffusion species. The overall photoconversion efficiencies of such devices could surpass those of conventional n-DSC device. Gibson et al. [40] have investigated a series of polyridyl cobalt complexes with different substituents as redox mediators in p-type DSC device, consisting of mesoporous NiO sensitized with a perylenemonoimide-naphthalenediimide (PMI-NDI) dyad. The devices' photocurrent and photovoltages were found to depend on the steric bulk of the redox species rather than their electrochemical potential. Nattestad et al. [41] have successfully applied the cobalt complex as redox mediator to fabricate p-n tandem cell, which showed promising results in improving on V_{oc}. Though the device shows low J_{sc} of only 0.97 mA/cm^2 and efficiency of 0.55%, the interesting V_{oc} value (0.91 V) matches relatively well the sum of the voltages delivered by each photoelectrode. These studies underscored the possibility to reach, in the future, higher voltages when new p-SC photocathodes or new electrolytes will be used.

5 Current and future developments

Recently study on new organic redox couples, such as disulfide/thioalte based shuttle, has shown promising potential for DSC application. Although the power conversion efficiencies of DSC devices have demonstrated over 12.3%, it is still too low compared to other technologies such as multi- junction collectors where efficiencies over 41% have been registered. These efficiencies differences are vast, so that at this moment DSC devices' main advantages are related to the simplicity of the fabrication and the promise of

a low cost technology. In order to fascinate the commercialization of DSC device, more research should be undertaken to improve the power conversion efficiencies in order to turn this technology into a very competitive option in worldwide photovoltaic solar cells market. For commercial application, cell efficiencies higher than 15% and module efficiencies higher than 10% are desired. To attain these values, both J_{sc} and V_{oc} must be further improved. Improvement has not yet reached the optimal value, which is mainly attributed to charge recombination between injected electrons and redox ions, and large over-potentials for redox shuttles. New sensitizers to suppress charge recombination and new redox couples or hole transport material are desired to improve device performance.

This work was supported by the Swiss National Science Foundation, the National Basic Research Program of China (2011CBA00703), the National Natural Science Foundation of China (20903030, 201173091), the Natural Science Foundation of Hubei Province (2011CDB0.4), the Talents Recruitment Program of HUST and the Program for New Century Excellent Talents in University (NCET-10-0416), and the Fundamental Research Funds for the Central Universities (HUST: 2011TS021). We thank Professors Yibing Cheng, Wei Chen and Zhixin Zhao at the HUST, and Dr. Shaik Zakeeruddin at the EPFL for fruitful discussion.

1 Shah A, Torres P, Tscharner R, et al. Photovoltaic technology: The case for thin-film solar cells. Science, 1999, 285: 692–698
2 Würfel P. Physics of Solar Cells: From Basic Principles to Advanced Concepts. Weinheim: Wiley-VCH, 2005
3 O'Regan B, Grätzel M. A low-cost, high-efficiency solar cell based on dye-sensitized colloidal TiO_2 films. Nature, 1991, 353: 737–740
4 Wang Y, Wu J, Lan Z, et al. Preparation of porous nanoparticle TiO_2 films for flexible dye-sensitized solar cells. Chin Sci Bull, 2011, 56: 2649–2653
5 Xiao Y, Wu J, Li Q, et al. Preparation of photoanode and its application to flexible dye-sensitized solar cells. Chin Sci Bull, 2010, 55: 980–985
6 Nazeeruddin M, Rodicio A, Humpbry-Baker R, et al. Conversion of light to electricity by cis-X2Bis(2,2′-bipyridyl-4,4′-dicarboxylate) ruthenium(II) charge-transfer sensitizers (X = Cl^-, Br^-, I^-, CN^-, and SCN^-) on nanocrystalline TiO_2 electrodes. J Am Chem Soc, 1993, 115: 6382–6390
7 Boschloo G, Hagfeldt A. Characteristics of the iodide/triiodide redox mediator in dye-sensitized solar cells. Accounts Chem Res, 2009, 42: 1819–1826
8 Grätzel M. Dye-sensitized solar cells. J Photochem Photobiol C-Photochem Rev, 2003, 4: 145–153
9 Nazeeruddin M, Humphry-Baker R, Liska P, et al. Investigation of sensitizer adsorption and the influence of protons on current and voltage of a dye-sensitized nanocrystalline TiO_2 solar cell. J Phys Chem B, 2003, 107: 8981–8987
10 Snaith H, Schmidt-Mende L. Advances in liquid-electrolyte and solid-state dye-sensitized solar cells. Adv Mater, 2007, 19: 3187–3200
11 Xie G X, Lin J M, Wu J H, et al. Application of upconversion luminescence in dye-sensitized solar cells. Chin Sci Bull, 2011, 56: 96–101
12 Chiba Y, Islam A, Watanabe Y, et al. Dye-sensitized solar cells with conversion efficiency of 11.1%. Jpn J Appl Phys Part 2, 2006, 45: L638–L640
13 O'Regan B, Durrant J. Kinetic and energetic paradigms for dye-sensitized solar cells: Moving from the ideal to the real. Accounts Chem Res, 2009, 42: 1799–1808
14 Nazeeruddin M, De Angelis F, Fantacci S, et al. Combined experimental and DFT-TDDFT computational study of photoelectrochemical cell ruthenium sensitizers. J Am Chem Soc, 2005, 127: 16835–16847
15 Bessho T, Zakeeruddin S M, Yeh C Y, et al. Highly efficient mesoscopic dye-sensitized solar cells based on donor-acceptor-substituted porphyrins. Angew Chem-Int Edit, 2010, 49: 6646–6649
16 Imahori H, Umeyama T, Ito S. Large π-aromatic molecules as potential sensitizers for highly efficient dye-sensitized solar cells. Accounts Chem Res, 2009, 42: 1809–1818
17 Wu S L, Lu H P, Yu H T, et al. Design and characterization of porphyrin sensitizers with a push-pull framework for highly efficient dye-sensitized solar cells. Energy Environ Sci, 2010, 3: 949–955
18 Chen C Y, Wu S J, Wu C G, et al. A ruthenium complex with superhigh light-harvesting capacity for dye-sensitized solar cells. Angew Chem-Int Edit, 2006, 45: 5822–5825
19 Lu H P, Mai C L, Tsia C Y, et al. Design and characterization of highly efficient porphyrin sensitizers for green see-through dye-sensitized solar cells. Phys Chem Chem Phys, 2009, 11: 10270–10274
20 Gao F, Wang Y, Shi D, et al. Enhance the optical absorptivity of nanocrystalline TiO_2 film with high molar extinction coefficient ruthenium sensitizers for high performance dye-sensitized solar cells. J Am Chem Soc, 2008, 130: 10720–10728
21 Papageorgiou N. Counter-electrode function in nanocrystalline photoelectrochemical cell configurations. Coord Chem Rev, 2004, 248: 1421–1446
22 Hamann T, Ondersma J W. Dye-sensitized solar cell redox shuttles. Energy Environ Sci, 2011, 4: 370–381
23 Hamann T, Jensen R, Martinson A, et al. Advancing beyond current generation dye-sensitized solar cells. Energy Environ Sci, 2008, 1: 66–78
24 Halme J, Vahermaa P, Miettunen K, et al. Device physics of dye solar cells. Adv Mater, 2010, 22: E210–E234
25 Shen Y, Nonomura K, Schlettwein D, et al. Photoelectrochemical kinetics of eosin Y-sensitized zinc oxide films investigated by scanning electrochemical microscopy. Chem-Eur J, 2006, 12: 5832–5839
26 Nusbaumer H, Zakeeruddin S M, Moser J E, et al. An alternative efficient redox couple for the dye-sensitized solar cell system. Chem-Eur J, 2003, 9: 3756–3763
27 Feldt S, Gibson E, Gabrielsson E, et al. Design of organic dyes and cobalt polypyridine redox mediators for high-efficiency dye-sensitized solar cells. J Am Chem Soc, 2010, 132: 16714–16724
28 Bai Y, Zhang J, Zhou D, et al. Engineering organic sensitizers for iodine-free dye-sensitized solar cells: Red-shifted current response concomitant with attenuated charge recombination. J Am Chem Soc, 2011, 133: 11442–11445
29 Li T, Spokoyny A, She C, et al. Ni(III)/(IV) bis(dicarbollide) as a fast, noncorrosive redox shuttle for dye-sensitized solar cells. J Am Chem Soc, 2010, 132: 4580–4582
30 Spokoyny A, Li T, Farha O, et al. Electronic tuning of Nickel-based bis(dicarbollide) redox shuttles in dye-sensitized solar cells. Angew Chem-Int Edit, 2010, 49: 5339–5343
31 Gregg B, Pichot F, Ferrere S, et al. Interfacial recombination processes in dye-sensitized solar cells and methods to passivate the interfaces. J Phys Chem B, 2001, 105: 1422–1429
32 Daeneke T, Kwon T H, Holmes A, et al. High-efficiency dye-sensitized solar cells with ferrocene-based electrolytes. Nat Chem, 2011, 3: 211–215
33 Wang M, Grätzel C, Moon S, et al. Surface design in solid-state dye sensitized solar cells: Effects of zwitterionic co-adsorbents on photovoltaic performance. Adv Funct Mater, 2009, 19: 2163–2172
34 Yue G T, Wu J H, Xiao Y M, et al. Flexible dye-sensitized solar cell based on PCBM/P3HT heterojunction. Chin Sci Bull, 2011, 56: 325–330
35 Snaith H, Zakeeruddin S, Wang Q, et al. Dye-sensitized solar cells incorporating a "liquid" hole-transporting material. Nano Lett, 2006, 6: 2000–2003
36 Wang M, Chamberland N, Breau L, et al. An organic redox electrolyte to rival triiodide/iodide in dye-sensitized solar cells. Nat Chem,

2010, 2: 385–389
37 Tian H, Yu Z, Hagfeldt A, et al. Organic redox couples and organic counter electrode for efficient organic dye-sensitized solar cells. J Am Chem Soc, 2011, 133: 9413–9422
38 Tian H, Jiang X, Yu Z, et al. Efficient organic-dye-sensitized solar cells based on an iodine-free electrolyte. Angew Chem-Int Edit, 2010, 49: 7328–7331
39 Ning Z, Tian H, Yuan C, et al. Solar cells sensitized with type-II ZnSe-CdS core/shell colloidal quantum dots. Chem Commun, 2011, 47: 1536–1538
40 Gibson E, Smeigh A, Le Pleux L, et al. A p-type NiO-based dye-sensitized solar cell with an open-circuit voltage of 0.35 V. Angew Chem-Int Edit, 2009, 48: 4402–4405
41 Nattestad A, Mozer A J, Fischer M, et al. Highly efficient photocathodes for dye-sensitized tandem solar cells. Nat Mater, 2010, 9: 31–35